On the impact of a more realistic physical layer on MANET simulations results

Illya Stepanov *, Kurt Rothermel

Department of Distributed Systems, Institute of Parallel and Distributed Systems, Universität Stuttgart, Universitätsstr. 38, 70569 Stuttgart, Germany

Received 14 October 2005; received in revised form 30 August 2006; accepted 31 August 2006
Available online 27 September 2006

Abstract

Network simulation tools are frequently used to analyze the performance of MANET protocols and applications. Currently they offer only simple wireless communication models that neglect many radio propagation effects. In this paper, we

Keywords: Communication systems; Mobile communication; UHF propagation; Geographic information systems; Simulation

1. Introduction

Mobile ad-hoc networks (MANETs) are created spontaneously by wireless communication peers, without relying on a fixed infrastructure. The devices communicate directly with each other when they are in transmission range. Common communication technologies are Bluetooth [23] and IEEE 802.11 [26]. Special ad-hoc routing algorithms are used for multi-hop communication. Many MANET applications exist, e.g., [2,12,20].

Network simulation tools [3,21,31] are frequently used to analyze the performance of MANET protocols and applications. These tools model the applications running on mobile devices, the wireless network protocol stack, radio signal propagation, and mobility of network users.

The radio propagation models used in common MANET simulators assume an obstacle-free area and a free line-of-sight between all communicating partners. As a consequence, the communication range is modeled by a circle around a mobile device. It is assumed that other devices residing within this

* Corresponding author. Tel.: +49 711 7816442; fax: +49 711 7816424.
E-mail addresses: illya.stepanov@informatik.uni-stuttgart.de (I. Stepanov), kurt.rothermel@informatik.uni-stuttgart.de (K. Rothermel).

Published in Ad Hoc Networks - Volume 6, Issue 1, January 2008, Pages 61-78

http://dx.doi.org/10.1016/j.adhoc.2006.08.001

circle receive the transmitted frames without errors. Communication with the devices beyond the circle is not possible. This approach poorly reflects radio wave propagation in a typical outdoor scenario, like a city center, in which buildings significantly affect communication between nodes. It does not consider transmission errors either. Nevertheless, the vast majority of publications that investigate MANET protocol and application behavior still relies on such simple models.

In this paper, we propose an improvement for the physical layer modeling in ns-2 [3], which is one of the most widely used network simulators. First, we integrate a more realistic radio propagation model. It uses ray tracing and considers geographic data of the simulation area. Such data are available from digital map vendors. The model has been evaluated against real-world measurements. Nevertheless, it requires more computation time. To cope with this problem, we precalculate possible sender–receiver path-loss values and store them in a database. Secondly, we add a model of wireless transmission errors. It estimates the packet bit-error rate from the received signal strength. The model is based on measurements of a card manufacturer at different transmission speeds [11]. We investigate progressively the impact of these changes on MANET simulation results.

The main contributions of this paper are following. We compare simulation results obtained with the commonly used physical layer models and a more realistic model. As metrics, we use the network connectivity and the performance of network protocols. We see significant difference between the results obtained with simple models and with a more realistic model. We also show that there are cases when simple models produce misleading simulation results.

The remainder of this paper is structured as follows. In Section 2, we describe the radio propagation models we use and their integration into ns-2. In Section 3, we describe the model of wireless transmission errors. Section 4 presents our simulation scenario. In Section 5, we compare the MANET topologies formed with different radio propagation models. Section 6 analyzes network partitioning. In Section 7, we compare the performance of network protocols. Section 8 shows how the fine-grained error model changes simulation results. In Section 9, we summarize our simulation results. Section 10 gives an overview of related work. Section 11 concludes our paper.

2. Radio propagation models and their integration into ns-2

In the following, we consider ns-2 as a MANET simulation tool [3], because it is adopted widely in the community. However, our general considerations are valid for most other tools as well.

Each time a mobile node transmits a frame in a simulation, ns-2 uses a propagation model to calculate the receive power of the radio signal for every potential receiving node. The frame is received without errors (0% bit-error rate) if the corresponding signal strength is not below the receive threshold of the network equipment (*RXThresh*). If the receive signal strength is below the receive threshold but it is above or equals the carrier-sense threshold (*CSThresh*), the frame is received with errors and is discarded. All frames with a power below the carrier sense threshold are ignored by the receiver. Two simultaneously arriving frames collide if the ratio of their signals is below the collision threshold (*CPThresh*).

Hence, the radio propagation model is the key factor to determine which nodes can communicate. It influences frame collisions and errors in a simulation. Obviously, to get realistic simulation results, it is essential to use a realistic radio propagation model.

2.1. Radio propagation models for outdoor scenarios

We consider radio propagation models for ultra-high frequency (UHF) communication technologies in outdoor environments. They can be classified into two major groups: empirical models and ray optical models. Empirical models come as formulas that provide estimations for the receive power based on the distance between the communication partners. Ray optical models use ray tracing or similar techniques to determine possible signal paths between the transmitter and the receiver in the given area. In this section, we first describe two empirical models, which are already integrated in ns-2 and therefore are commonly used in MANET simulations. Then, we present the "intelligent ray tracing" model, which provides more realistic results.

2.1.1. Combination of free space and two-ray ground models

The "free space" model was proposed by Friis [7]. It assumes exactly one path between the trans-

mitter and the receiver. The path must be clear from obstacles.

$$P_r = \frac{P_t G_t G_r \lambda^2}{(4\pi)^2 d^2 L} \quad (1)$$

where P_r is the received signal power (in W), P_t is the transmitted signal power, G_r and G_t are the gains of the receiving and the transmitting antennas respectively, λ is the wave length, L is the system loss, and d is the distance between the transmitter and the receiver.

According to [8], a single direct path between the communicating partners exists seldom at larger distances. The "two-ray ground" model considers both the clear path and the ground reflected path:

$$P_r = P_t G_t G_r \frac{h_t^2 h_r^2}{d^4 L} \quad (2)$$

In addition to the parameters of the free space model, the equation contains h_r and h_t, which are the heights of receiving and the transmitting antennas respectively. Similar to the free space model, the model neglects obstacles of the propagation environment.

However, the two-ray ground model is too optimistic for the short transmitter–receiver separation distances. Hence, in most applications, the two models are combined. The free space model is used at small distances, while the two-ray ground model is used at larger distances. The distance at which both models give identical results ($d_c = 4\pi h_t h_r/\lambda$) is used as cross-over distance.

The described combination of free space and two-ray ground models is the mostly used model in MANET research community.

2.1.2. Log-distance path-loss model

The "log-distance path-loss" model [8] expresses the decrease of the received power with distance raised to some exponent:

$$P_r = P_{r0}\left(\frac{d_0}{d}\right)^{\beta} \quad (3)$$

where: P_{r0} is the free space receive power at the close-in reference distance d_0, β is the path-loss exponent. Usually $d_0 = 1$ m.

The exponent β depends on the propagation environment. For the open-space area like in the free space model, $\beta = 2$. For urban areas with obstacles, β is between 2.5 and 3.5. Manufactures of wireless cards normally use $\beta = 2.7$ to specify the maximum transmission range for a typical outdoor environment (cf. [16]). In our paper, we use the log-distance path-loss model with $\beta = 2.5$, 2.7, 3.0 as another reference model.

2.1.3. Intelligent ray tracing model

The main advantage of the empirical models described above lies in their simplicity and therefore in their low computational complexity. However, since the distance between the sender and the receiver is the only dynamic parameter of these models, the communication area defined by $P_r \geqslant RXThresh$ is simply a circle. The models do not take the geographic environment into account. As depicted in Fig. 1, this poorly reflects the reality in urban environments.

Ray-optical models [22] use ray tracing (Fig. 2) to determine all possible signal paths between the transmitter and the receiver. They consider a geographic map of the simulation area. Reflection, diffraction, and scattering of radio waves are taken

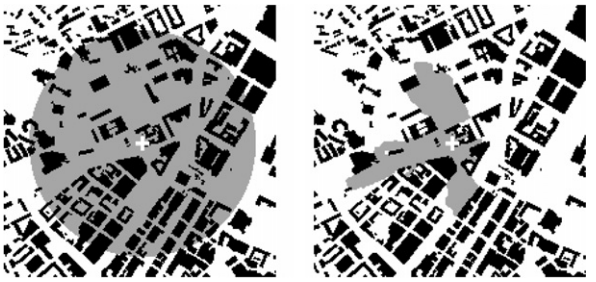

Fig. 1. Communication area of a WLAN node computed with the combined two-ray ground model (on the left) and the ray tracing model (on the right). The transmitter is partially blocked by buildings.

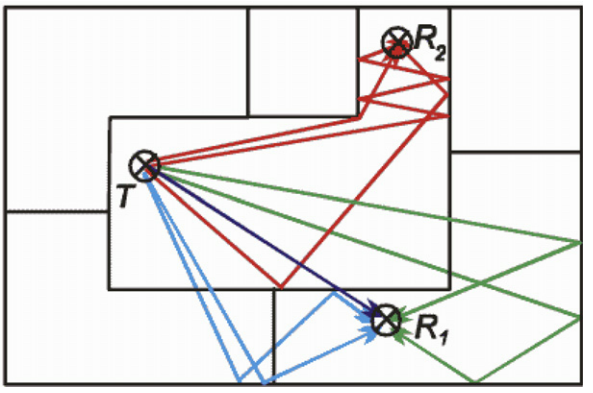

Fig. 2. Ray optical propagation paths between a transmitter and two receivers (taken from [10]).

into account. The components of individual paths are summed to obtain the receive signal power. The models provide accurate results, but require longer computation time.

In this paper, we use the "intelligent ray tracing" model [28], which is an improved version of the classic ray tracing approach. In order to accelerate the performance of ray tracing, the model preprocesses the digital map and computes visibility relations between walls, thus achieving the acceleration factor near 1000. The accuracy of the model is proven by measurements in European cities. Thus, for Helsinki (Finland), the mean error of predicted signal-loss results is close to 0 dB and the standard deviation is around 8 dB [19]. For Munich (Germany) and Nancy (France), the mean error is 0 dB and the standard deviation is less than 7 dB [27,28]. In this paper, we apply the intelligent ray tracing model in Stuttgart (Germany) city center, for which the mean error is 0.3 dB and the standard deviation is 5.8 dB [10,14].

2.2. Implementation

The simulation tool ns-2, which we use for our integration and sample measurements, already provides the combination of the free space and the two-ray ground models (called "two-ray ground model" for simplicity) and the log-distance path-loss model (called "shadowing model"). In the following, we describe how we integrate the intelligent ray tracing model into ns-2 [24].

We use a commercial implementation of the intelligent ray tracing model (WinPROP by AWE Communications [1,19]). As input, WinPROP requires a 2.5-dimensional geographic model of the target area. We extracted the necessary data from the digital map of Stuttgart city center (the whole area size is about 2.4 km × 1.9 km). For any given sender position (and other static parameters like sender height, transmission power, wavelength, etc.), WinPROP can calculate a map of receive power values for a grid, representing possible positions of a receiver. The algorithm implemented in WinPROP does not allow to calculate the receive power for just one receiver position efficiently. In our simulations, we use a 5 m × 5 m grid, which is the smallest grid size we could handle (smaller grid sizes would require much longer computation time and more disk space). We performed a separate investigation to assure that the chosen grid size has minor impact on simulation results.

Because it takes WinPROP about 30 s to calculate a receive power map for one sender position, it would not be sensible to call WinPROP every time ns-2 needs a receive power value; this would lead to several million calls for one simulation. Instead, we precalculated the receive power values for each possible sender–receiver pair in our scenario in a 5 m × 5 m grid. For our scenario size, this translates to about 32 billions of position pairs. The precalculation step took three days on a 50-node PC cluster and produced about 120 GB of output data (since we store each value in a 4-byte float). Once computed, the data are used till the next substantial change in the spatial environment (and in the corresponding digital map). We assume that those changes happen rather rarely. So the overhead for the precalculation will be typically amortized over many simulation runs. Currently, we need to recalculate the data from scratch in the case of any change in a spatial environment. In future, it should be possible to perform "smart update" by limiting the update area to the vicinity of change (similar as done by ns-2, which considers only the neighbors within *CSThresh*).

To use the calculated data with ns-2, we implemented our own radio propagation module. Each time ns-2 needs a receive power value, our module reads the appropriate value from the dataset. To reduce the data access overhead, our module implements a caching strategy. As the result, the overall ns-2 simulation time with our propagation module is comparable to the simulation time with an empirical model.

3. Fine-grained model of wireless transmission errors

ns-2 does not simulate other transmission errors except of checking if a frame's receive power is above or below the receive threshold of the network equipment. In order to make it more realistic, we integrate a fine-grained model of wireless transmission errors.

The model is based on measurements of a card manufacturer [11]. The measurements estimate bit-error rate from the signal-to-interference-and-noise ratio of received packet and the modulation scheme used at the given transmission speed. In IEEE 802.11b, the following modulation schemes are used: DBPSK at 1 Mbps, DQPSK at 2 Mbps, CCK5.5 at 5.5 Mbps, and CCK11 at 11 Mbps [26].

We use the implementation of the model from [29,30]. It models errors upon transmissions of both data and IEEE 802.11b control frames. The signal-to-interference-and-noise ratio (SINR, in dB) is calculated from the power of the received frame (P_r, in W), the powers of other frames at the receiver ($\sum_{i \neq r} P_i$, in W), and the receiver noise floor (P_0, in W):

$$\mathrm{SINR} = \frac{P_r}{P_0 + \sum_{i \neq r} P_i} \tag{4}$$

P_0 is about 10 dB below the receiver sensitivity specified by the manufacturer. The obtained signal-to-interference-and-noise ratio and the transmission speed are used as table indexes to determine the bit-error rate from the measured data.

4. Simulation scenario

To show the impact of the more realistic models on MANET simulation results, we use a typical simulation scenario (Table 1). A MANET is formed by pedestrians in Stuttgart city center (Fig. 3). We simulate scenarios with various numbers of PDA-equipped mobile users (from 10 to 300). For the modeling of user mobility, we use the "user-oriented mobility model" described in [25]. The movement area is constrained to the dense street network of Stuttgart downtown (1.5 km × 1.5 km). The coordinates of streets are taken from the same digital map as the building information. During the simulation, users execute random trips. The movement paths between trip points are obtained using the Dijkstra shortest-path algorithm [6]. Users move with a typical pedestrian speed between 2 and 5 km/h.

Table 1
Parameters of the simulation scenario

Simulation time	900 s
Transmission power (P_t)	15 dBm
Radio frequency	2.442 GHz
Transmission speed	1, 2, 5.5, 11 Mbps
Receive threshold (*RXThresh*)	−94, −91, −87, −82 dBm (depending on transmission speed)
Carrier-sense threshold (*CSThresh*)	−104 dBm
Collision threshold (*CPThresh*)	10 dB
System loss (L)	1
Antenna type	Omnidirectional
Antenna gain (G)	1
Antenna height (h)	1.5 m
Routing protocol	AODV
Data traffic	Constant-bit rate UDP traffic
Packet size	512 bytes
Data traffic intensity	1 packet/s

Fig. 3. Map of the simulation area.

In our scenario, the users are equipped with mobile devices. The devices communicate wirelessly using IEEE 802.11b. Since ns-2 only supports communication at a fixed transmission speed, we consider separately the four transmission speeds supported by IEEE 802.11b. We take the basic hardware parameters (transmission power and receive threshold) from hardware datasheets [16]. The carrier-sense threshold and the collision threshold, which are not directly specified by hardware manufacturers, are set to the values suggested in [30]. In the simulations with the fine-grained error model, we set the receive threshold to the carrier-sense threshold, so the frame reception is only determined from the error rate. We use the following radio propagation models: the two-ray ground model (TRG), the log-distance path-loss model with $\beta = 2.5,\ 2.7,\ 3.0$ (LG2.5, LG2.7, LG3.0, respectively) and the intelligent ray-tracing model (IRT).

To compare routing protocol performance, we simulate constant-bit rate UDP traffic between some users (5 connections between 8 users). Packet transmissions start at different times (between 5 and 150 s). One packet is sent every second. This communication pattern is used in all simulation runs. For multi-hop routing, we use ad-hoc on-demand distance vector routing (AODV) [17].

The presented results are obtained as an average after 20 simulation runs with different randomly generated mobility patterns.

5. Comparison of MANET topologies

First, we demonstrate the impact of the more realistic radio propagation model on MANET connectivity. To monitor the change in topologies in time, we use a custom event-based topology simulation tool in addition to ns-2. The tool determines for every pair of mobile nodes times when they enter or leave each other's transmission range (we do not consider transmission errors in this section). Thereby, we construct MANET topology graphs at different time steps.

5.1. Metrics

We apply our metrics to a directed topology graph. Graph edges represent possible connections

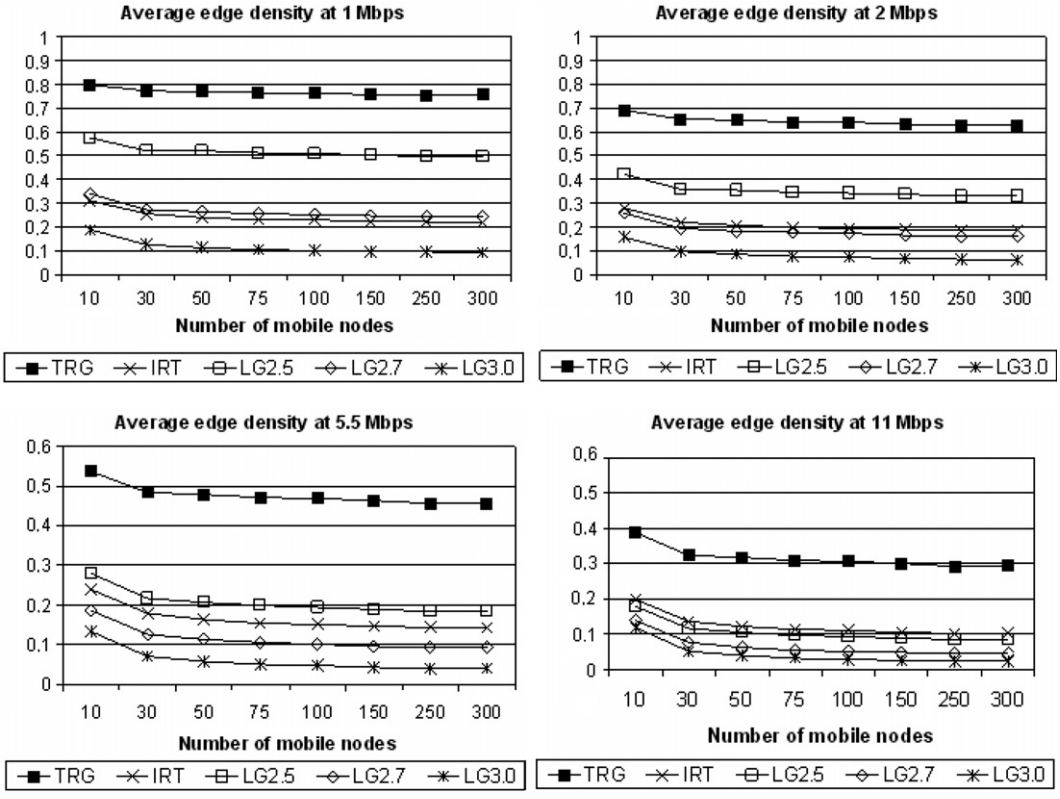

Fig. 4. Average edge density.

between mobile nodes. We consider that a node j is connected to a node i if it can receive transmissions from i with the signal power above the receive threshold. We assume that the edge $i \to i$ always exists.

Edge density in the MANET topology graph is a fraction of graph edges to the maximum number of graph edges. The edge density reflects how close the network graph to a "complete" graph is. In the complete graph, all the nodes are interconnected. Since $i \to i$ exists always, the metric takes values in $[1/N, 1]$, where N is the total number of mobile nodes in the scenario.

We use the *degree of dissimilarity* to express difference between two topology graphs. We represent a graph with the adjacency matrix $T(x_{ij})$, $i = 1, \ldots, N$, $j = 1, \ldots, N$, where x_{ij} is a bit value of 1 if the edge $i \to j$ exists, and 0 otherwise. Then *hamming distance* between two matrices is the number of elements that the matrices differ on. The degree of dissimilarity is a fraction of the hamming distance to the sum of edges in both graphs. The metric points out a ratio of dissimilar edges in both graphs. Since we consider $i \to i$ always exists, it takes values between 0 and $(N^2 - N)/(N^2 + N)$, where the latter corresponds to the case when two graphs have only $i \to i$ connections in common.

In the charts, we present the *weighted average* of results. So, we aggregate individual results by taking into account the relevance of each component, which is the duration of time that the network connectivity graph was in the particular state.

5.2. Results

Average edge density (AED) in graphs (Fig. 4) changes slightly with a number of mobile nodes. Hence, it is a good metric for comparing radio propagation models at different node densities. At all transmission speeds, $\mathrm{AED_{TRG}} > \mathrm{AED_{LG2.5}} > \mathrm{AED_{LG2.7}} > \mathrm{AED_{LG3.0}}$, which is expected, since the network connectivity decreases with the decrease of transmission range. For the same reason, AED is lower at higher transmission speeds. The high values of TRG AED at 1 and 2 Mbps point up dense graphs, in which a number of edges roughly quadratic in their number of vertices. In such networks, a large group of nodes resides in the same collision domain, which leads to frequent contentions upon simultaneous

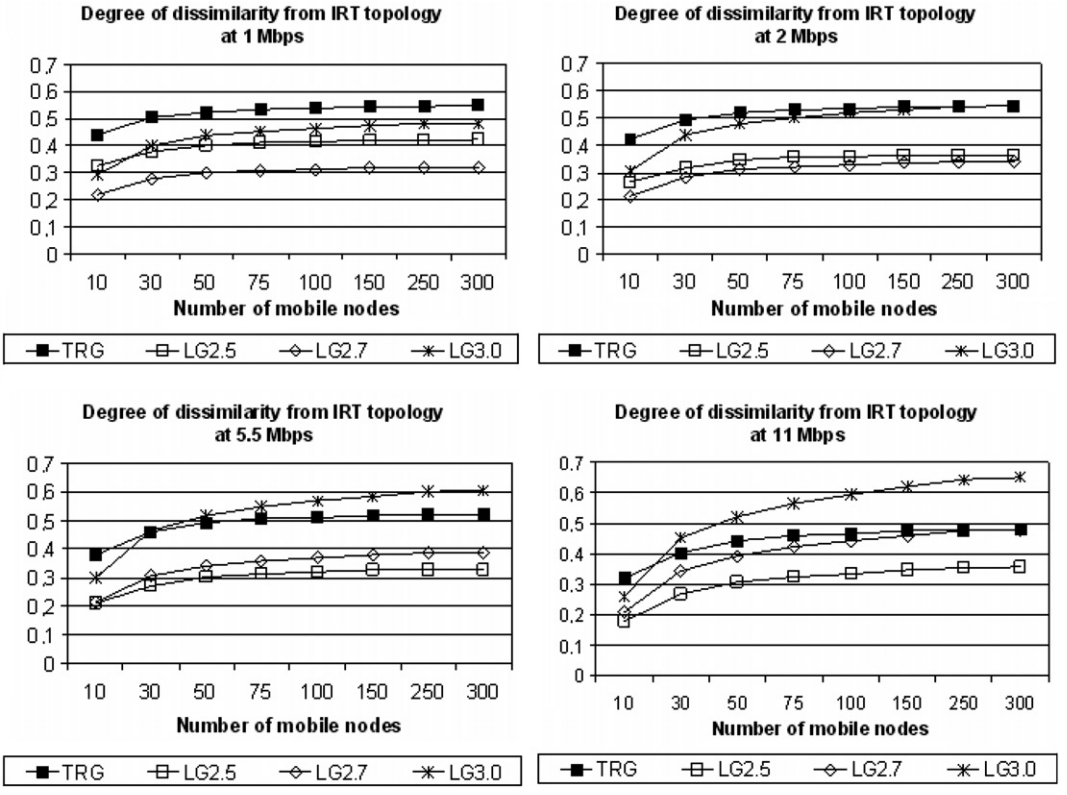

Fig. 5. Degree of dissimilarity from IRT topology.

transmissions. At all transmission speeds, the IRT graphs remain sparse disregarding the number of mobile nodes. The graphs of LG2.7 at 1, 2 Mbps and LG2.5 at 5.5, 11 Mbps have the closest to IRT average edge density.

The degree of dissimilarity (Fig. 5) shows significant difference between the topologies created with IRT and empirical models. Depending on the model and the transmission speed, the topologies differ on 20–70% of edges. At 1 and 2 Mbps, the graphs of LG2.7 are the closest to IRT with a difference in about 30% of edges. At 5.5 and 11 Mbps, LG2.5 is the closest with a difference in about 30–35%.

We performed a detailed investigation to determine where the difference comes from. Thus, at 1 Mbps, the difference is about 13% of IRT edges that are missing in LG2.7 and about 18% of LG2.7 edges that are missing in IRT. At 2 Mbps, the ratios of distinct edges are 20% and 13%, respectively. At 5.5 Mbps, about 10% of IRT edges are missing in LG2.5 and about 20% of LG2.5 edges are missing in IRT. At 11 Mbps, about 20% of distinct edges exist in IRT and about 13% are in LG2.5.

The results of our detailed investigation show that:

(a) The edges that are missing in IRT are those blocked by communication obstructions. Mainly from these edges comes a difference in topologies between IRT and the models with relatively long transmission ranges, like TRG.
(b) Some edges exist only in IRT and are missing in LG topologies. As shown in Fig. 1, IRT and TRG have equal transmission range in a free space area. By applying the LG model with β greater than 2, we decrease transmission range in order to reflect the propagation in obstructed areas. However, we then underestimate propagation in open areas. The difference between IRT and LG3.0 comes mainly from such edges.

Thus, although some empirical models manage to create topologies with almost the same number of possible network connections, the topologies

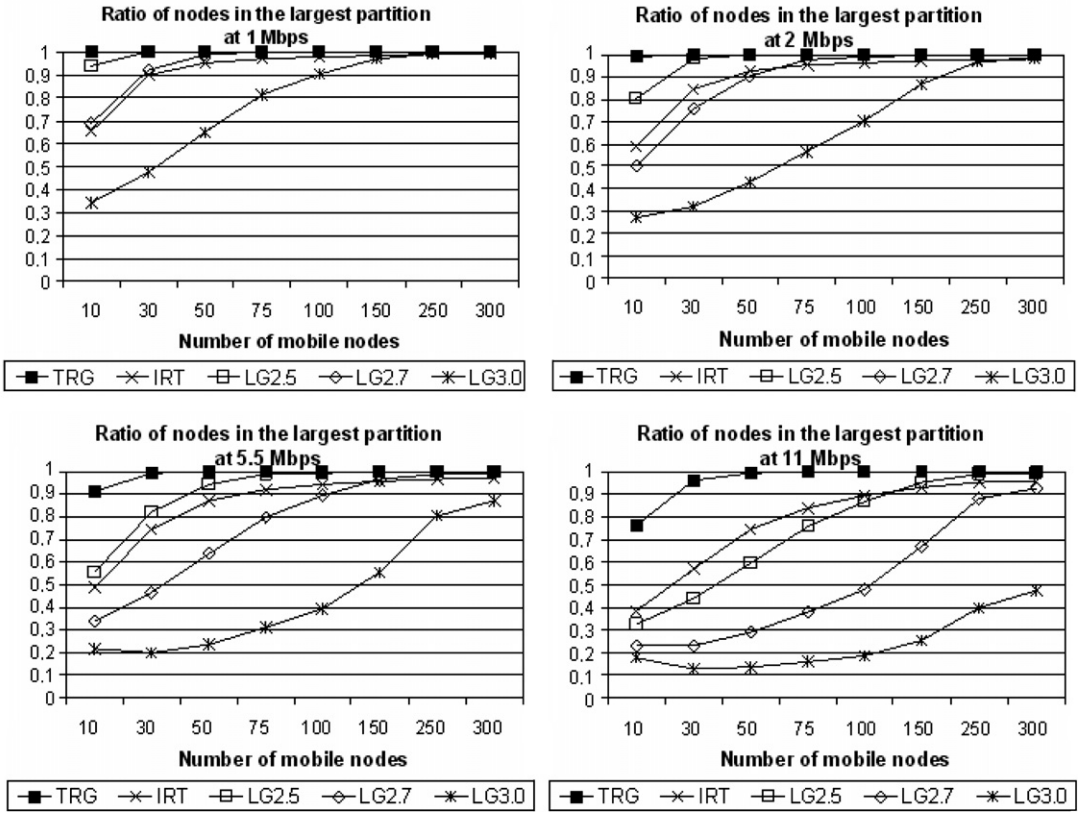

Fig. 6. Ratio of nodes in the largest partition.

differ significantly from IRT. At lower transmission speeds, the difference mainly comes from the edges existing in empirical models. At higher transmission speeds, more distinct connections exist in IRT. The commonly used TRG model produces dense topologies at 1 and 2 Mbps. The IRT graphs remain sparse at all transmission speeds.

6. Comparison of network partitioning

Network partitioning impacts significantly performance of network applications. In this section, we analyze the impact of the more realistic radio propagation models on partitioning. Similar to the previous section, we use a custom event-based topology modeling tool for monitoring changes in time.

6.1. Metrics

Number of partitions corresponds to the number of isolated groups of nodes. The communication is possible only among the nodes belonging to the same group. *Ratio of nodes in the largest partition* is a fraction of nodes residing in the largest partition to the total number of mobile nodes in the scenario.

In the charts, we present the *weighted average* of results. We aggregate individual results by taking into account the relevance of each component, which is the duration of time that the network connectivity graph was in the particular state.

6.2. Results

For all propagation models, the ratio of nodes in the largest partition (Fig. 6) increases with the number of mobile nodes. For most models, at large node densities, nearly 100% of nodes are in the largest partition. The results of LG2.7 at 1, 2 Mbps and LG2.5 at 5.5, 11 Mbps are the closest to IRT.

The results of the average number of network partitions (Fig. 7) show two main issues of simple empirical models. First, when the network connectivity is very low (e.g., with LG3.0 model at 11 Mbps), the number of partitions increases with the number of mobile nodes. We basically get many

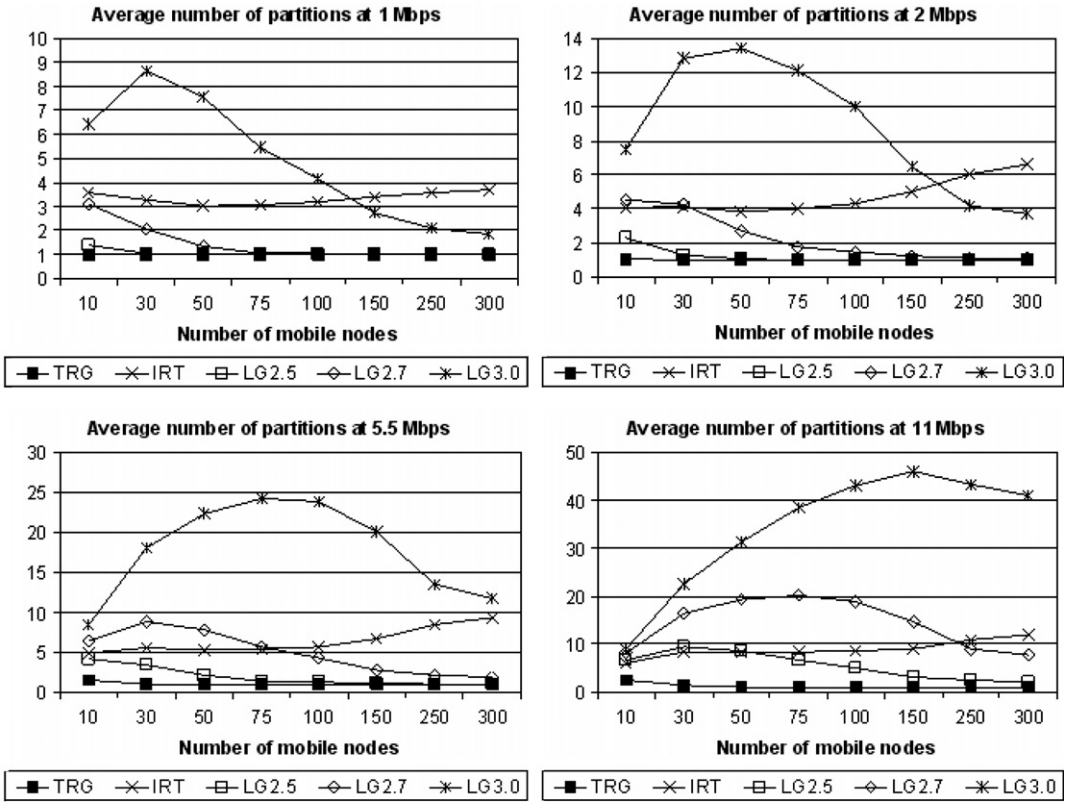

Fig. 7. Average number of partitions.

isolated nodes distributed in the area. Secondly, starting from certain node densities, the number of partitions decreases, which is the expected behavior.

Contrariwise, for IRT model, the number of partitions constantly increases with the number of mobile nodes. By taking the ratio of nodes in the largest partition into account, we see that these partitions are formed by isolated single nodes or small groups of nodes. They occur because of communication obstacles, which simple empirical models cannot reflect. Hence, it is a unique property of the more realistic model.

7. Impact of radio propagation models on MANET protocol performance

In this section, we investigate how the more realistic radio propagation model impacts performance of MANET protocols. Here we only compare different radio propagation models without considering the fine-grained model of transmission errors.

7.1. Metrics

Data packet delivery ratio is the ratio between the number of data packets successfully delivered to recipients and the number of data packets originated by constant-bit rate (CBR) sources. *Routing packet overhead* is the ratio between the number of routing packets and the total number of packets sent. *Data packet delay* is the time elapsed from the data packet origination at a source and its delivery to the recipient. *Hop count* is the number of nodes that a data packet traversed to the recipient. It is important to note that these two metrics consider only the packets successfully delivered to recipients.

In the charts below, we present the *geometric average* (the *n*th root of the product of *n* terms) of the simulation results obtained from 20 randomly generated mobility patterns.

7.2. Results

Data packet delivery ratio (DR) (Fig. 8) increases with the number of mobile nodes. This happens due

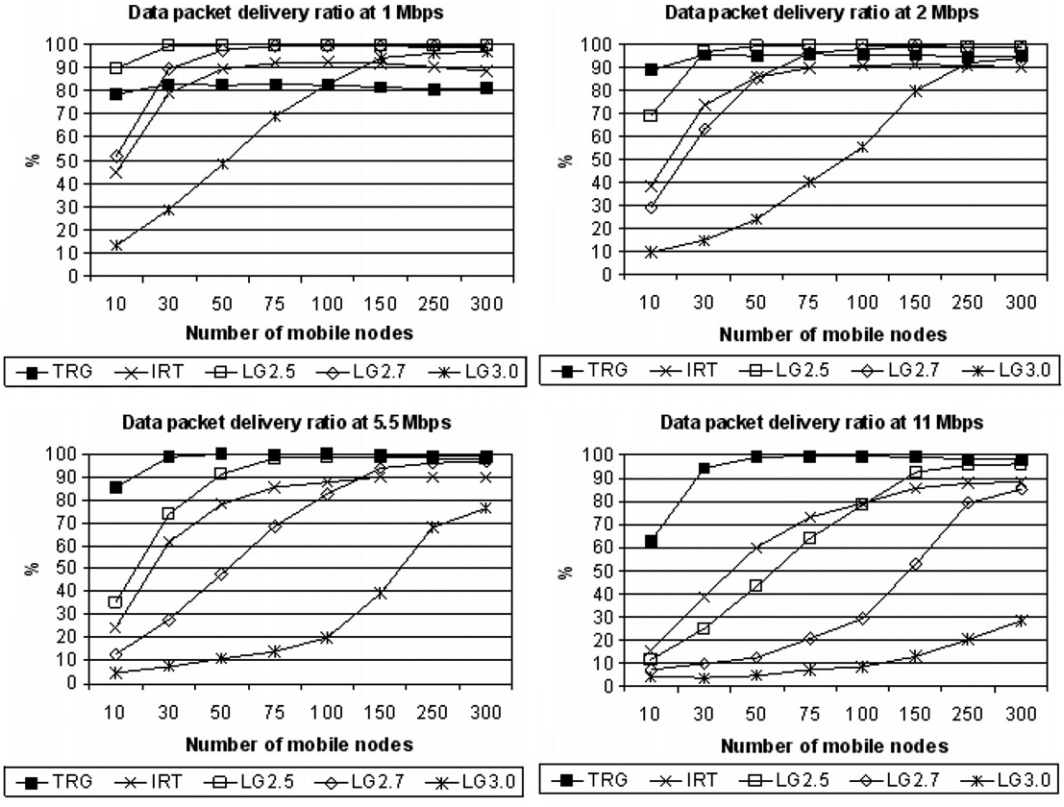

Fig. 8. Average data packet delivery ratio.

to the increase in the network connectivity and the decrease in the network partitioning, which we observe in previous sections. Also because of the network connectivity, $DR_{TRG} > DR_{LG2.5} > DR_{LG2.7} > DR_{LG3.0}$. The exceptions are 1 and 2 Mbps, when TRG delivers unexpectedly fewer packets in comparison to other models. The reason behind is that AODV uses flooding to find a route to destination. In dense (as of Fig. 4) networks, this leads to frequent packet collisions when multiple nodes initiate route discoveries. The results of LG2.7 at 1, 2 Mbps and LG2.5 at 5.5, 11 Mbps are the closest to IRT.

Routing packet overhead (PO) is shown in Fig. 9. Since more routing packets are required in less-connected networks for route search and maintenance, $PO_{TRG} < PO_{LG2.5} < PO_{LG2.7} < PO_{LG3.0}$. The routing overhead also increases with the number of mobile nodes. This happens because more routing packets are sent while the number of data packets remains almost constant. Again, the exceptions are 1 and 2 Mbps, when TRG shows high routing overhead. This is due to repetitive packet retransmissions occurring in densely connected networks. At all transmission speeds, IRT shows nearly the highest routing packet overhead. This occurs because of obstacles, which stress route search and maintenance.

The number of hops traversed by data packets (HC) is shown in Fig. 10. At lower node densities, it slightly increases with the number of mobile nodes. Then it stays constant. It is important to note that the results of simulations with less than 30% data packets delivered are not representative, since the number of samples is small. In such simulations, most of the packets are delivered between nearby nodes. Due to the observed network connectivity, $HC_{TRG} < HC_{LG2.5} < HC_{LG2.7} < HC_{LG3.0}$. The results of LG2.7 at 1 Mbps and LG2.5 at 2 Mbps are very close to IRT. At 2 Mbps, the IRT results are between LG2.5 and LG2.7. At 11 Mbps, the IRT results are between TRG and LG2.5.

The results of data packet delay (PD) are shown in Fig. 11. Because of the observed data path lengths and extra overhead for route discovery, $PD_{TRG} < PD_{LG2.5} < PD_{2.7} < PD_{LG3.0}$. For the same radio propagation model, the delay decreases with

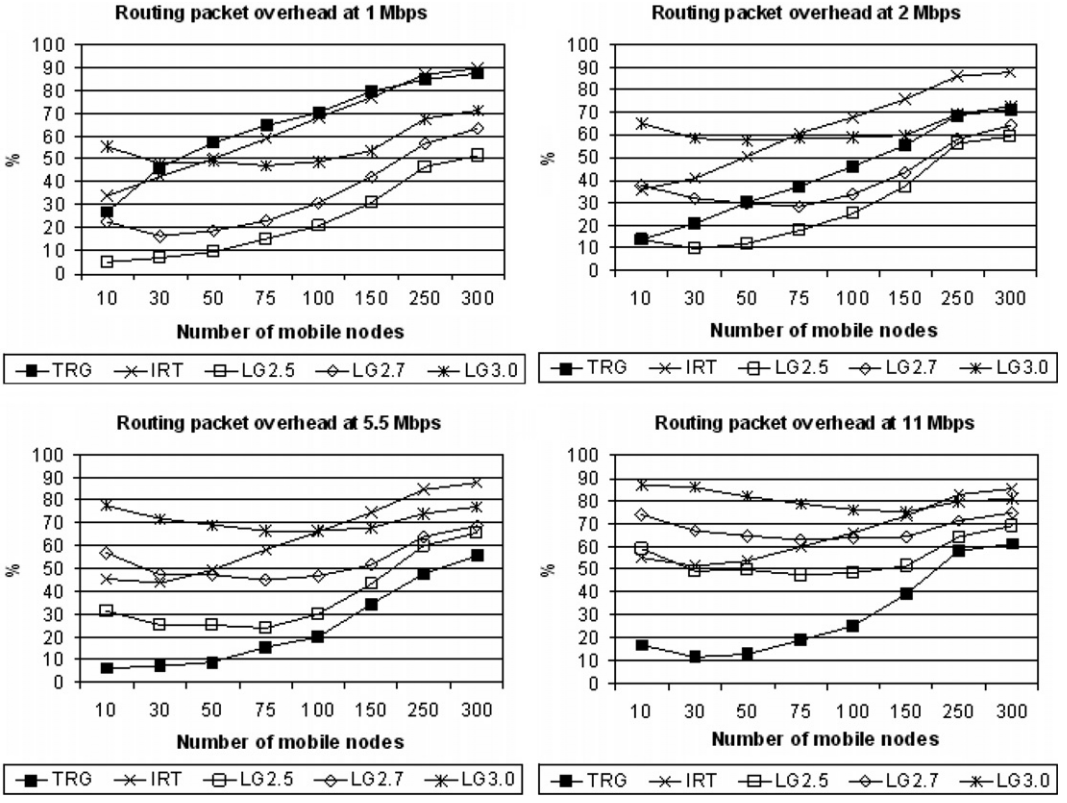

Fig. 9. Routing overhead.

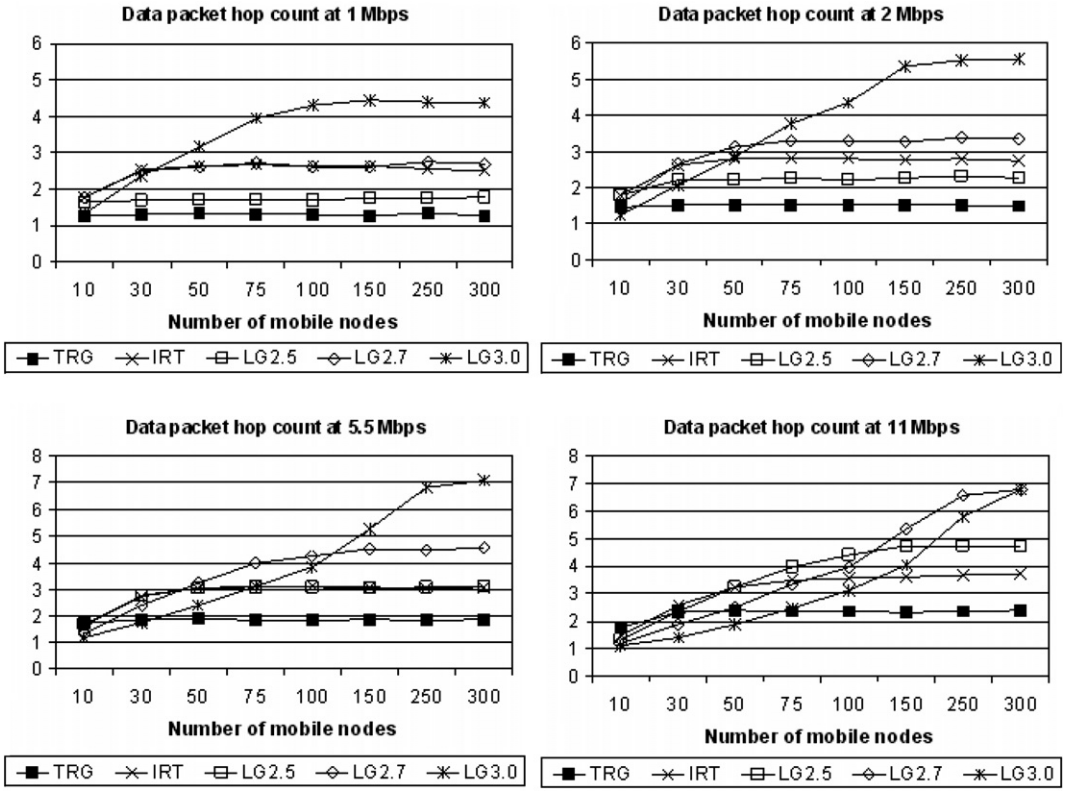

Fig. 10. Data packet hop count.

the increase of transmission speed from 1 to 5.5 Mbps. However, the delay increases at 11 Mbps. Here, route discovery and maintenance in a less-connected network takes more time that what is gained by a faster transmission speed. Then it stays constant. Again, the results of simulations with less than 30% data packets delivered are not representative, since the number of samples is small.

For IRT model at 1 and 2 Mbps, the observed data packet delay is between the results of LG2.7 and LG3.0. LG2.7 at 5.5 Mbps and LG2.5 at 11 Mbps are the closest to IRT. With a consideration of path lengths, we see that the extra delay for IRT model is contributed by additional route discovery and maintenance overhead.

Hence, we see quantitative differences in results obtained with IRT model. Since the model is more realistic, we claim that our results are more accurate than those obtained with simple empirical models. LG2.7 at 1, 2 Mbps, LG2.5 at 5.5, 11 Mbps are close to IRT according to some metrics like data packet delivery ratio or data packet hop count. Nevertheless, routing overhead is much higher with IRT model. This is due to obstacles, which stress route search and maintenance.

8. Impact of fine-grained error model on MANET simulation results

In this section, we demonstrate how a more realistic fine-grained model of transmission errors changes simulation results.

8.1. Metrics

For comparisons, we use the same metrics as in the previous section: data packet delivery ratio, routing packet overhead, data packet delay, and data packet hop count.

8.2. Results

Simulation results are shown in Figs. 12–15. The general behavior of the curves is similar to Figs. 8–11. except the following key differences.

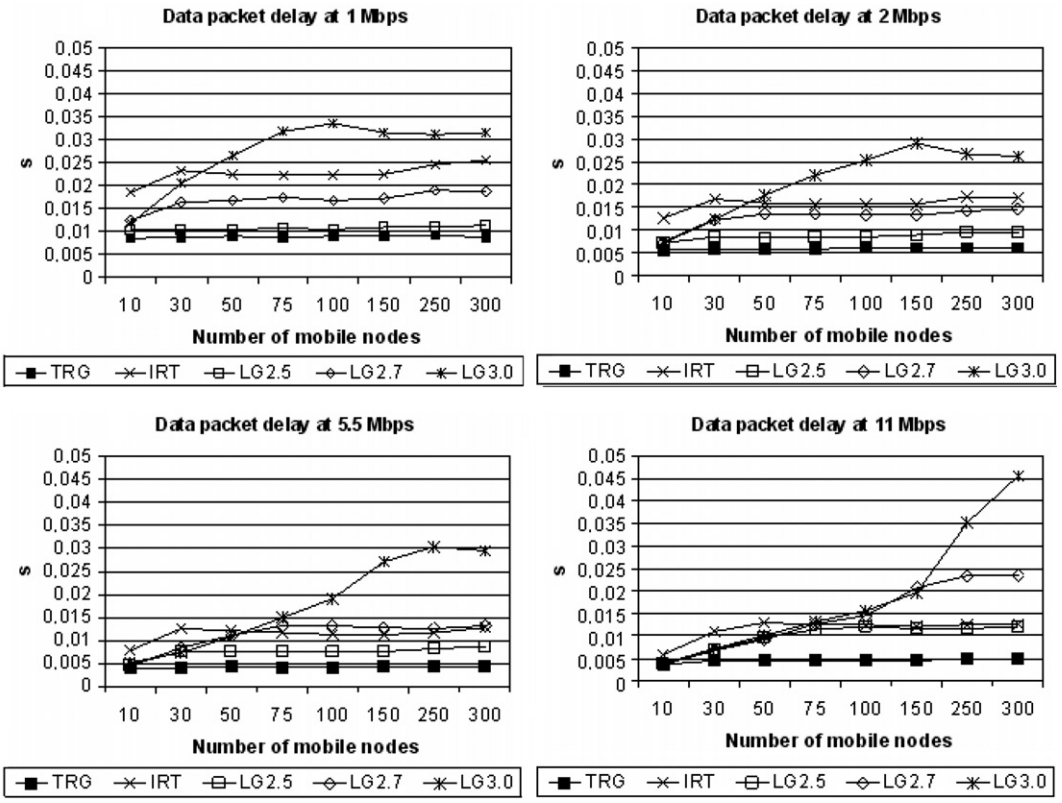

Fig. 11. Data packet delay.

TRG simulations do not suffer from massive collisions at 1 and 2 Mbps any more (Figs. 12 and 13). Detailed analysis of trace files shows that the modeled transmission errors reduce the number of nodes within the same collision domain that are involved in AODV route discovery. We see significant performance degradation in LG simulations with $\beta > 2.5$ at 5.5 and 11 Mbps (Fig. 12). There are less than 50% of packets delivered even in scenarios with 300 mobile nodes.

The fine-grained error model increases routing overhead (Fig. 13). For IRT model, it is quite moderate in comparison to other models. Also the lengths of routing paths (Fig. 14) and end-to-end packet delay (Fig. 15) increase.

In general, the fine-grained error model stresses MANET performance. It leads to the decrease of packet delivery ratio, increase of routing overhead, routing paths, and end-to-end packet delay. At 1 and 2 Mbps, the results of data packet delivery ratio, routing overhead, and packet delay in LG2.7 simulations are the closest to IRT. Hop count in IRT simulations is close to LG2.5. At 5.5 and 11 Mbps, IRT results are between TRG and LG2.5.

9. Simulation summary

We demonstrated that a more realistic physical layer model changes simulation results considerably. The ray tracing model produces connection topologies that differ on 20–70% of edges. At lower transmission speeds, the difference mainly comes from the connections existing in empirical models, which do not consider communication obstructions. At higher speeds, more distinct connections exist in the simulations with the ray tracing model. We also got additional partitions formed by single or small groups of nodes, which appear because of communication obstacles. As of some routing protocol performance metrics, the log-distance path-loss model with $\beta = 2.7$ at 1, 2 Mbps and with $\beta = 2.5$ at 5.5, 11 Mbps is the closest to ray tracing model. The reason behind is that the corresponding network topologies are the closest to IRT. The difference comes from both sides: some edges exist only in IRT, some

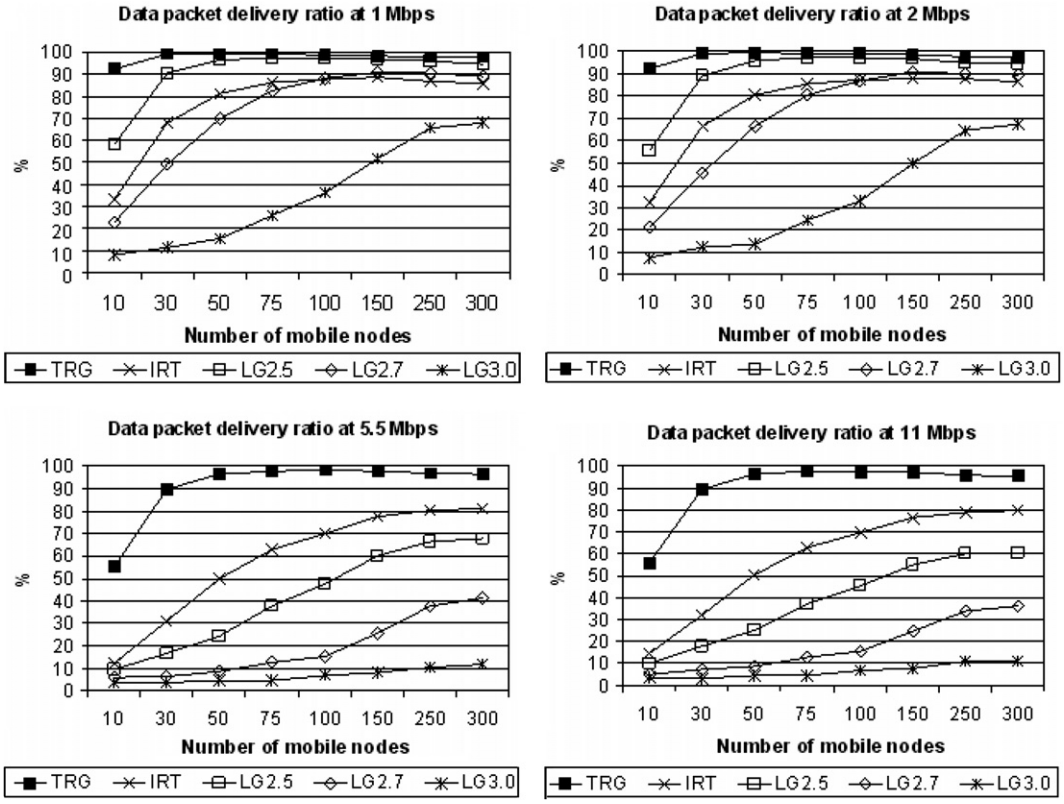

Fig. 12. Average data packet delivery ratio with the fine-grained error model.

edges exist only in LG. After computing an average over a large number of packets, the results are somewhat close. The difference between IRT and TRG and between IRT and LG3.0 comes only from one side. This makes the performance results differ more even after computing an average over a large number of packets. The reflection of obstacles requires more routing packets to be sent in simulations with a more realistic model. The two-ray ground model which is commonly used in MANET simulations produces dense topology graphs at 1 and 2 Mbps. This causes unrealistic packet collisions, which in turn leads to misleading simulation results (i.e., lower packet delivery ratio and much higher routing overhead even in comparison to LG2.5 and LG2.7, which is not observed with a more realistic model).

The applied fine-grained model of wireless transmission errors reduced the number of nodes within the same collision domain, which are involved in AODV route discovery. It led to more reasonable simulation results with the two-ray ground model. The error model stresses routing protocol performance, thus decreasing data packet delivery ratio and increasing routing overhead, data path lengths, and end-to-end packet delay. We saw significant performance degradation in LG simulations with $\beta > 2.5$ at 5.5 and 11 Mbps. The routing overhead in simulations with the ray tracing model is quite moderate in comparison to other models. The results of log-distance path-loss model with $\beta = 2.7$ are the closest to ray tracing model at 1 and 2 Mbps. At 5.5 and 11 Mbps, the results of ray tracing model are between the results of two-ray ground model (which is basically the log-distance path-loss model with $\beta = 2$) and log-distance path-loss model with $\beta = 2.5$.

10. Related work

A detailed statistics in [15] about the publications at premium conferences in the field proves that the papers with simple radio propagation models outnumber others significantly. Most authors are only interested in a comparative performance analysis of their protocols and applications, like in [4]. For their studies, they use open-space areas without

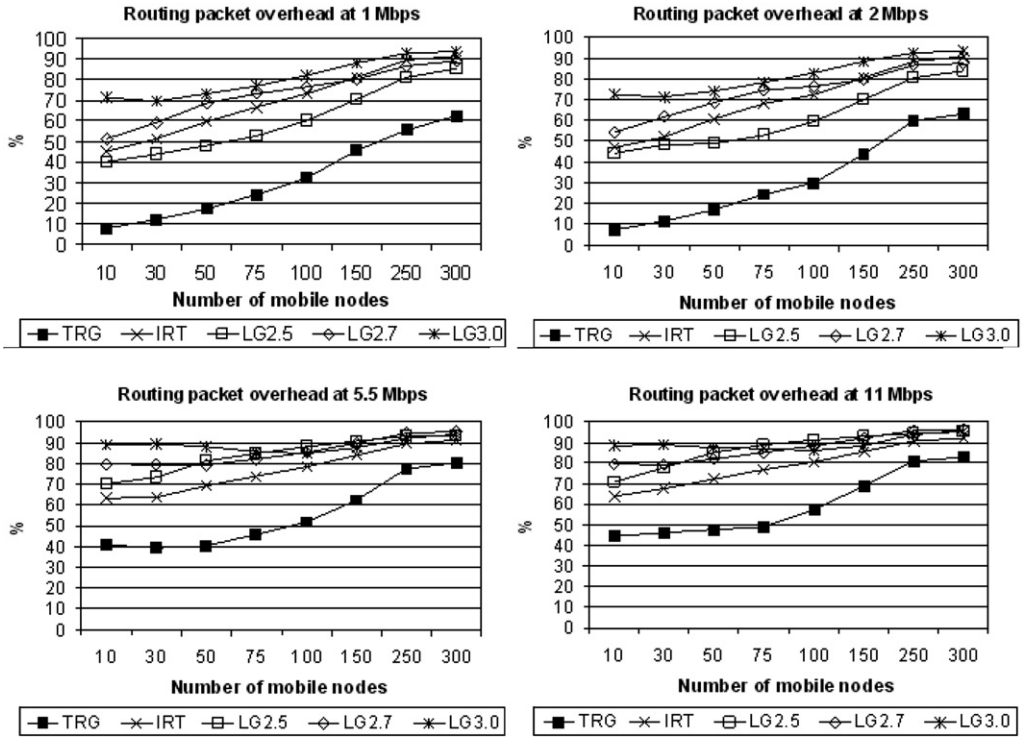

Fig. 13. Routing packet overhead with the fine-grained error model.

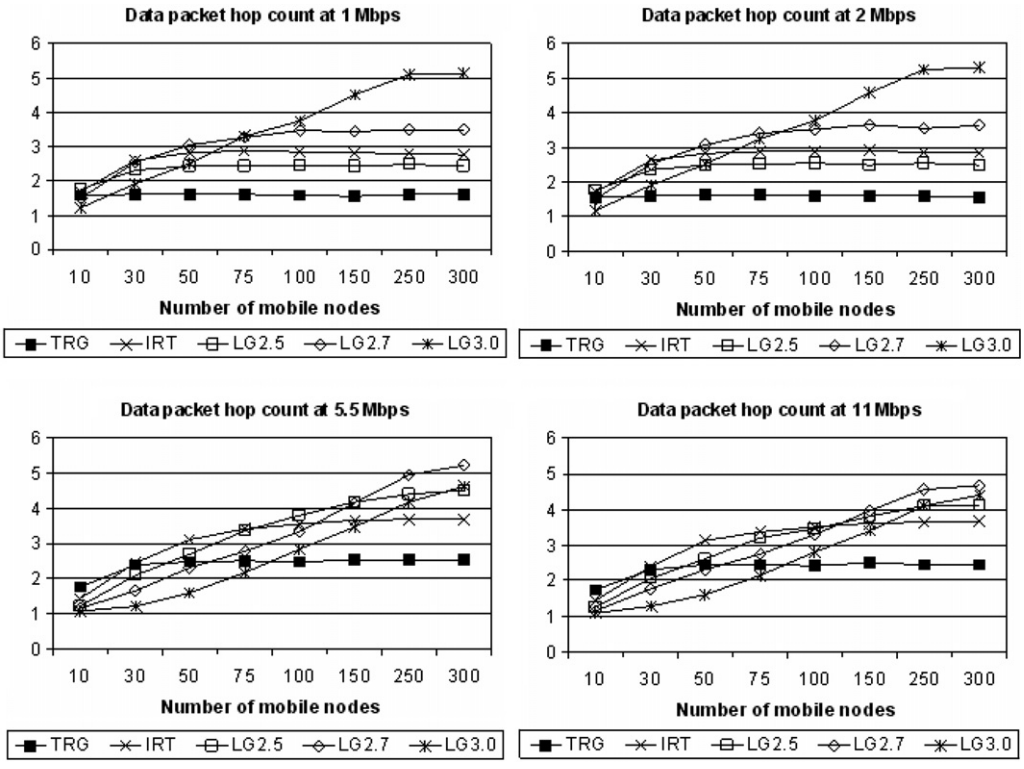

Fig. 14. Data packet hop count with the fine-grained error model.

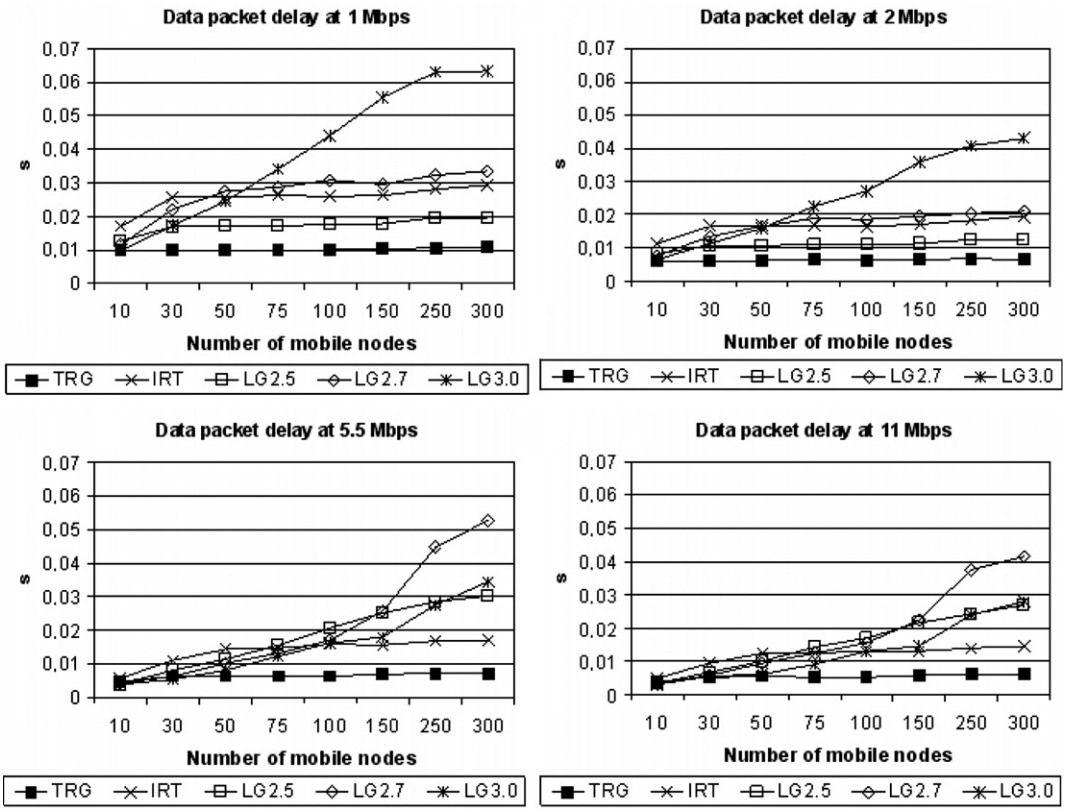

Fig. 15. Data packet delay with the fine-grained error model.

obstacles and simplified assumptions about transmission errors.

The widely used MANET simulation tools ns-2 [3], GloMoSim [31], and GTNetS [21] offer only the free space model and the two-ray ground model. In addition, ns-2 provides the shadowing model, which is basically the log-distance path-loss model extended with a random term.

In [13], the authors consider communication obstructions of a simulation area. They assume a communication between two nodes is not possible if a direct path between them is blocked with an obstacle. The authors agree that this approach is a too simple workaround, since it neglects multipath propagation of radio waves.

In [9], the authors make a step towards improving the radio propagation modeling for MANET simulations. They integrate the empirical COST–Walfisch–Ikegami model [5] into ns-2 simulation environment. Besides other parameters of empirical radio propagation models, this model considers the heights of the transmitter and the receiver, mean building height, mean width of roads, mean building separation, and road orientation with respect to the direct radio path. Clearly, the Walfisch–Ikegami model is more realistic than other empirical models that do not consider geographic information at all. However, ray tracing models are much more realistic as they also reflect the propagation paths in the horizontal plane.

Transmission errors are reflected seldom in MANET simulations. Like this paper, [18,30] also rely on measurements from [11]. However, the authors use them with simple empirical models.

11. Conclusion

In this paper, we proposed an improvement for the physical layer modeling in outdoor scenarios for ns-2. It consists of a more realistic radio propagation model and a fine-grained model of wireless transmission errors, which have been evaluated against real-world measurements. Our simulations showed significant difference between the real connection topologies and the topologies obtained with simple models that are currently offered by MANET

simulation tools. The obtained protocol performance results might be similar as of some metrics, however they differ in other. We also saw that there are cases when simple models even produce misleading results (e.g., the two-ray ground model at 1 and 2 Mbps causes a huge number of collisions without the fine-grained transmission error model, or the log-distance path-loss model with $\beta > 2.5$ at 5.5 and 11 Mbps leads to a poor network performance, which is not observed with more realistic models). Hence, since the simple models cannot capture many realistic radio propagation effects, more realistic models must be used for the MANET performance evaluation in the concrete area. We showed that such models can be integrated into ns-2.

Acknowledgments

We thank Philipp Wertz (Institute of Radio Frequency Technology, Universität Stuttgart) and Hermann Buddendick (AWE Communications) for their support regarding the radio propagation software. We thank reviewers for their valuable comments and suggestions.

References

[1] AWE Communications Home Page. Available from: <http://www.awe-communications.com>.

[2] C. Becker, M. Bauer, J. Hähner, Usenet-on-the-fly: supporting locality of information in spontaneous networking environments, in: Proceedings of CSCW 2002 Workshop on Ad hoc Communications and Collaboration in Ubiquitous Computing Environments, New Orleans, USA, 2002.

[3] L. Breslau, D. Estrin, K. Fall, S. Floyd, J. Heidemann, A. Helmy, P. Huang, S. McCanne, K. Varadhan, Y. Xu, H. Yu, Advances in network simulation, IEEE Computer 33 (5) (2000) 59–67.

[4] J. Broch, D. Maltz, D. Johnson, Y. Hu, J. Jetcheva, A performance comparison of multi-hop wireless ad hoc network routing protocols, in: Proceedings of the 4th Annual ACM/IEEE International Conference on Mobile Computing and Networking (MobiCom'98), Dallas, USA, October 1998, pp. 85–97.

[5] COST-231, Urban transmission loss models for mobile radio in the 900- and 1800 MHz bands, Revision 2, September 1991.

[6] E. Dijkstra, A note on two problems in connection with graphs, Numerische Mathematik 1 (1959) 269–271.

[7] H. Friis, A note on a simple transmission formula, in: Proceedings of IRE, vol. 41, 1946, pp. 254–256.

[8] J. Gibson, The Communications Handbook, CRC Press, 1997, ISBN 0849383498.

[9] I. Gruber, O. Knauf, H. Li, Performance of ad hoc routing protocols in urban environments, in: Proceedings of European Wireless 2004 (EW'2004), Barcelona, Spain, February 2004.

[10] R. Hoppe, P. Wertz, F.M. Landstorfer, G. Wölfle, Advanced ray optical wave propagation modelling for urban and indoor scenarios including wideband properties, European Transactions on Telecommunications (ETT) 1 (November) (2003) 61–69.

[11] Intersil® HFA3861B Direct Sequence Spread Spectrum Baseband Processor Data Sheet. File Number 4816, January 2000.

[12] J. Jetcheva, Y.-C. Hu, S. PalChaudhuri, A. Saha, D. Johnson, Design and evaluation of a metropolitan area multitier wireless ad hoc network architecture, in: Proceedings of the 5th IEEE Workshop on Mobile Computing Systems & Applications, Monterey, USA, October 2003.

[13] P. Johansson, T. Larsson, N. Hedman, B. Mielczarek, M. Degermark, Scenario-based performance analysis of routing protocols for mobile ad-hoc networks, in: Proceedings of the 5th ACM/IEEE International Conference on Mobile Computing and Networking (MobiCom'99), Seattle, USA, August 1999, pp. 195–206.

[14] R. Hoppe, G. Wölfle, F. Landstorfer, Fast 3D ray tracing for the planning of microcells by intelligent preprocessing of the database, in: Proceedings of the 3rd European Personal and Mobile Communications Conference (EPMCC) 1999, Paris, France, March 1999.

[15] D. Kotz, C. Newport, R. Gray, J. Liu, Y. Yuan, C. Elliott, Experimental evaluation of wireless simulation assumptions, in: Proceedings of the ACM/IEEE International Symposium on Modeling, Analysis and Simulation of Wireless and Mobile Systems (MSWiM'04), Venice, Italy, October, 2004, pp. 78–82.

[16] Orinoco® 11b Client PC Card Specification. Available from: <www.proxim.com>.

[17] C. Perkins, E. Royer, Ad hoc on-demand distance vector routing, in: Proceedings of the 2nd IEEE Workshop on Mobile Computing Systems and Applications, New Orleans, USA, February 1999, pp. 90–100.

[18] J. del Prado, S. Choi, Link adaptation strategy for IEEE 802.11 WLAN via received signal strength measurement, in: Proceedings of the 38th Annual IEEE International Conference on Communications (ICC), Anchorage, USA, May 2003, pp. 1108–1113.

[19] T. Rautiainen, G. Wölfle, R. Hoppe, Verifying path-loss and delay spread predictions of a 3D ray tracing propagation model in urban environments, in: Proceedings of the 56th IEEE Vehicular Technology Conference (VTC) 2002 – Fall, Vancouver, Canada, September 2002, pp. 2470–2474.

[20] D. Reichardt, M. Miglietta, L. Moretti, P. Morsink, W. Schulz, CarTALK 2000 – Safe and comfortable driving based upon inter-vehicle-communication, in: Proceedings of IEEE Intelligent Vehicle Symposium, Versailles, France, June 2002, vol. 2, pp. 545–550.

[21] G. Riley, The Georgia Tech Network Simulator, in: Proceedings of ACM SIGCOMM Workshop on Models, Methods and Tools for Reproducible Network Research (MoMeTools'03), Germany, August 2003, pp. 5–12.

[22] K. Schaubach, N. Davis IV, T. Rappaport, A ray tracing method for predicting path-loss and delay spread in microcellular environments, in: Proceedings of the 42nd IEEE Vehicular Technology Conference (VTC) 1992, Denver, USA, May 1992, pp. 932–935.

[23] Specification of the Bluetooth System Ver. 1.1, Bluetooth SIG, 2001.
[24] I. Stepanov, D. Herrscher, K. Rothermel, On the impact of radio propagation models on MANET simulation results, in: Proceedings of the 7th IFIP International Conference on Mobile and Wireless Communications Networks (MWCN 2005), Marrakech, Morocco, September 2005.
[25] I. Stepanov, P. Marron, K. Rothermel, Mobility modeling of outdoor scenarios for MANETs, in: Proceedings of the 38th Annual Simulation Symposium (ANSS'38), San Diego, USA, April 2005, pp. 312–322.
[26] Wireless LAN Medium Access Control (MAC) and Physical Layer (PHY) Specifications, IEEE Standard 802.11b, 1999.
[27] G. Wölfle, B. Gschwendtner, F. Landstorfer, Intelligent ray tracing – a new approach for the field strength prediction in microcells, in: Proceedings of the 47th vehicular technology conference (VTC), Phoenix, USA, May 1997, pp. 790–794.
[28] G. Wölfle, R. Hoppe, F. Landstorfer, A fast and enhanced ray optical propagation model for indoor and urban scenarios, based on an intelligent preprocessing of the database, in: Proceedings of the 10th IEEE International Symposium on Personal, Indoor and Mobile Radio Communications (PIMRC), Osaka, Japan, September 1999.
[29] X. Wu, Simulate 802.11b channel within ns2, Technical Report, National University of Singapore, Singapore, 2004.
[30] X. Wu, A. Ananda, Link characteristics estimation For IEEE 802.11 DCF based WLAN, in: Proceedings of the 29th Annual IEEE Conference on Local Computer Networks (LCN 2004), Tampa, USA, November 2004, pp. 302–309.
[31] X. Zeng, R. Bagrodia, M. Gerla, GloMoSim: a library for parallel simulation of large-scale wireless networks, in: Proceedings of the 12th Workshop on Parallel and Distributed Simulations (PADS'98), Banff, Canada, May 1998, pp. 154–161.